Damaging Southerly Winds Caused by Barrier Jets in the Cook Strait and Wellington Region of New Zealand

YANG YANG, MICHAEL UDDSTROM, MIKE REVELL, STUART MOORE, AND RICHARD TURNER

National Institute of Water and Atmospheric Research, Wellington, New Zealand

(Manuscript received 28 April 2016, in final form 1 December 2016)

ABSTRACT

Strong southerly winds regularly occur in the Cook Strait region of New Zealand. Occasionally, these winds are strong enough to cause severe damage to property and threaten human life. One example of a storm containing such winds is the ''Wellington Storm,'' which occurred on 20 June 2013. For this case, wind speeds in Cook Strait were stronger than those observed or forecast elsewhere in the storm. Even though wind speeds of this intensity are rare, storms affecting New Zealand with central pressures equal to the Wellington Storm (~976 hPa) are not uncommon. Numerical experiments have been carried out to investigate the possible reasons for the exceptional damaging southerly winds (DSWs) occurring in this storm. Analyses of the simulations showed that DSWs in Cook Strait for this event were actually barrier jets, not gap winds as they appeared. The strength of barrier jets in Cook Strait is sensitive to the precise location of the storm center. This explains the uncommon occurrence of DSWs in Cook Strait. Numerical experiments that used scaled (either increased or decreased) New Zealand orography showed that the barrier jets became shallower and weaker when the mountain top heights were lower. This decrease in barrier jet strength with mountain height is largely consistent with the results from linear-scale analyses in previous publications. This result implies that numerical simulations using a lower topography than actual (usually the case in current operational NWP) may lead to errors in timing and in forecasting the strength of the damaging winds associated with barrier jets.

1. Introduction

The interaction of mountains with environmental airflow often leads to localized high winds such as barrier jets, gap winds, and downslope storms. Gap winds are winds downstream of mountain gaps, stronger than adjacent airflows (Pan and Smith 1999). A distinctive feature of the gap wind is that its speed exceeds the upstream wind speed due to acceleration from higher upstream pressure to lower downstream pressure.

Downslope winds may occur in the lee of mountains when air is forced to flow over them (Durran 2003). In suitable atmospheric conditions, downslope winds have been found to occur at many locations [e.g., the Rocky Mountain chinook (Lilly 1978), the southern Alpine foehn in New Zealand (Yang et al. 2012)], and can develop to be severe (wind speed $>20\,\mathrm{m\,s^{-1}}$). Two main theories have been put forward to explain these severe downslope winds: (i) resonant amplification (Clark and Peltier 1984; Scinocca and Peltier 1993) and (ii) the hydraulic theory (Smith 1985).

A barrier jet, on the other hand, is a strong low-level mountain-parallel flow on the windward side due to mountain blocking (Schwerdtfeger 1975; Parish 1982; Overland and Bond 1993). Adiabatic ascent of airflow on the windward side of a mountain (Mass and Ferber 1990) leads to the occurrence of a cold anomaly and positive pressure perturbation against a mountain barrier. A barrier jet is developed as the winds accelerate down the along-barrier pressure gradient on the windward side.

The occurrence and development of barrier jets depends on the strength and stability of the upstream airflow and on the shape and height of the mountain range. According to Overland and Bond (1995) and Pierrehumbert and Wyman (1985), the Burger number is defined as $B = (N/f)(h_m/L)$, where $N\,[=\sqrt{(g/\theta)(\partial\theta/\partial z)}\,]$, h_m, f, and L are the Brunt–Väisälä frequency (referred to as N hereafter), the effective mountain height, the Coriolis parameter, and the mountain half-width, respectively. For $B > 1$, the mountain ridge is wall-like

Corresponding author e-mail: Dr. Yang Yang, y.yang@niwa.co.nz

DOI: 10.1175/MWR-D-16-0159.1

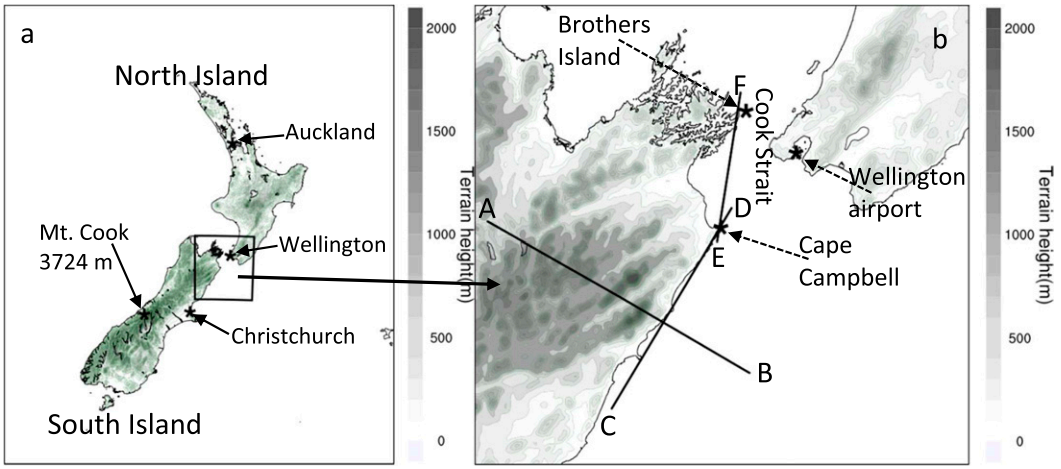

FIG. 1. (a) NZCSM domain covering New Zealand and the three cities denoted by ★ symbols. (b) The Cook Strait, mountains (shading), positions of cross sections (lines AB, CD, and EF), and locations of three stations (denoted by ★ symbols) used in this study.

and the mountain-parallel momentum balance is ageostrophic [i.e., low-level winds accelerate down the along-barrier pressure gradient; Overland and Bond (1993, 1995)]. Barrier jets have been found to occur frequently in places where the Burger number is normally greater than 1 [e.g., the Appalachians (Richwien 1980; Bell and Bosart 1988), east of the Rocky Mountains (Colle and Mass 1995), the Sierra Nevada (Marwitz 1983; Neiman et al. 2011), and in the European Alps (Bousquet and Smull 2003a,b), as well as along the coasts of California–Oregon (Yu and Smull 2000), the southern Alaskan coast (Olson et al. 2007), and the west coast of Taiwan (Li and Chen 1998; Yeh and Chen 2003)]. Barrier jets also frequently occur along the west coast of the South Island of New Zealand, parallel to the Southern Alps (Revell et al. 2002).

New Zealand consists of two main islands: North Island and South Island. The South Island is dominated by mountain ranges with a southwest–northeast orientation, known as the Southern Alps with a peak mountain height of 3724 m, at Mt. Cook (Fig. 1a). The North and South Islands are separated by Cook Strait (Fig. 1b) with a width of about 20–60 km. The Wellington region is located in the southwest of the North Island. Reid (1996) analyzed pressure values at mean sea level (MSL) at a few stations in the region of Cook Strait for a 2-yr period and found that winds have directions approximately parallel to the pressure gradient.

Damaging southerly winds (DSWs) occurred during a storm that impacted the Cook Strait and coastal Wellington area in the evening of 20 June 2013. Storms such as this one, hereafter referred to as the "Wellington Storm," are not uncommon in New Zealand in terms of the minimum mean sea level pressure in the storm (~976 hPa); however, the exceptionally strong winds and damage caused by the Wellington Storm on the night of 20 June were unusual. For example, at Brothers Island to the west of Cook Strait (Fig. 1b), the maximum southerly gust wind speed reached 51 m s^{-1} at 0900 UTC (Fig. 2). The maximum southerly wind speed observed at Wellington Airport on the evening of 20 June was ~40 m s^{-1} (Fig. 2), the strongest for the past 20 years (not shown). The hourly maximum gusts at Cape Campbell were stronger than at Wellington Airport but weaker than at Brothers Island when DSWs occurred in Cook Strait. Large trees were downed and transmission line pylons and roofs were damaged, with the greatest damage levels in the south coast region of Wellington.

From simulations using the New Zealand Convective Scale Model (NZCSM), it is interesting to note that stronger surface southerly winds (>30 m s^{-1}) than elsewhere in the storm were found mainly in the Cook Strait and Wellington coastal region (Fig. 3). However, it was not clear as to which of, if any (or combination of) the three mountain-related effects was responsible for the DSWs. Numerical simulations of this storm have been carried out to investigate the mechanisms behind these localized DSWs, and the effects of mountain heights and environmental incoming airflow directions on barrier jet strength.

The paper is structured as follows: a description of the synoptic weather situation and the numerical model and data used is presented in section 2; factors leading to the DSWs are analyzed in sections 3 and 4, respectively; and results from sensitivity experiments exploring the sensitivity of barrier jets to mountain heights and incoming

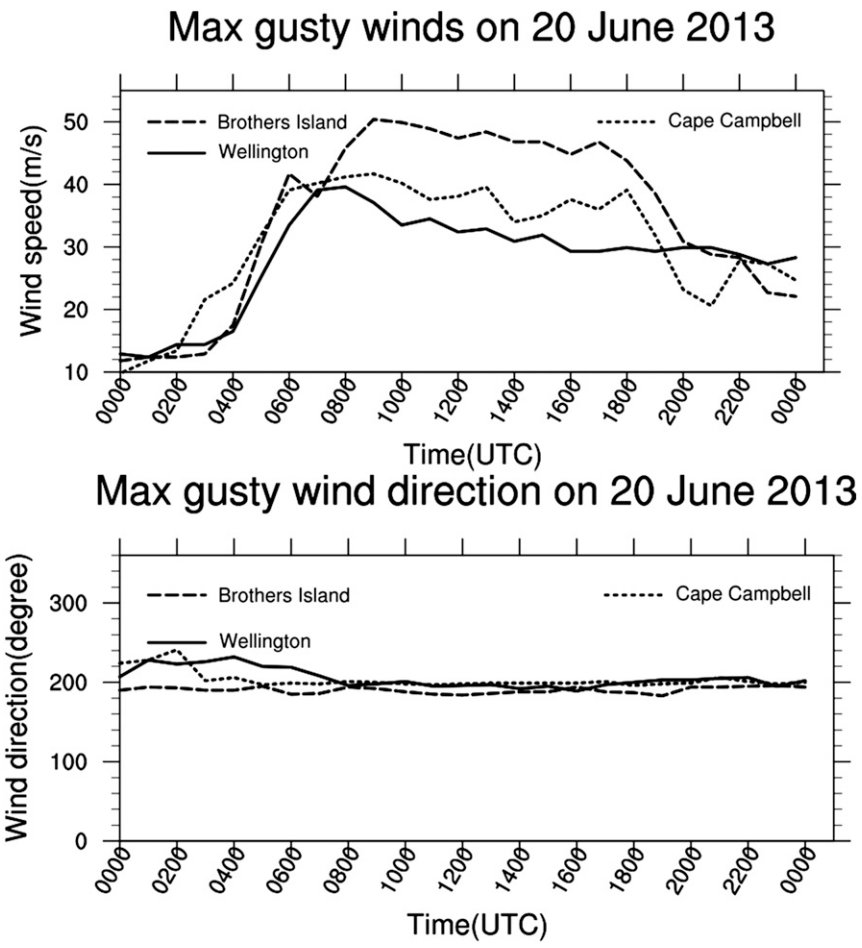

FIG. 2. Observed hourly maximum gust (top) wind speed and (bottom) direction at the Wellington Airport, Cape Campbell, and Brothers Island (Fig. 1b).

airflow directions are analyzed in sections 5 and 6. Finally, a short summary is given in section 7.

2. Description of weather, model, and data

a. Weather

The Wellington Storm moved eastward from the Australian continent and intensified quickly over the Tasman Sea. At 0600 UTC 14 June 2013, the main body of a low pressure system was located off the east coast of Australia with a central pressure of ~1000 hPa (Fig. 4a). At 0600 UTC 16 June, the central pressure decreased to ~996 hPa and started to affect New Zealand with surface northeasterly winds predominating across the country. At 0600 UTC 18 June, the low showed two pressure minima at the surface: one was over the central Tasman Sea (~992 hPa) and the other was to the southeast of the South Island (~989 hPa). At 0600 UTC 20 June, the central pressure further decreased to 976 hPa (Fig. 4d) and was located to the west of the North Island.

This low exhibited a baroclinic structure typical of other midlatitude cyclones during its development stage as illustrated by simulations with the New Zealand Limited Area Model (NZLAM) (Webster et al. 2003; Yang et al. 2011, 2012). For example, at 0600 UTC 16 June 2013 at 500 hPa (Fig. 5a), higher temperatures were found to the east of the low center with warm advection and lower temperatures to the west of the low with cold advection. At 0600 UTC 20 June when DSWs affected the Cook Strait and Wellington region, the low center at 500 hPa coincided with the center of the upper-level cold air and the associated cold/warm advection was much weaker than before (Fig. 5b), indicating that by this stage baroclinic conversion of potential to kinetic energy were playing less of a role in the development of the low. In addition, the maximum Ertel potential vorticity (PV) associated with the low on the isentropic surface of 310 K showed a dramatic increase from approximately −5 PVU (1 PVU = 10^{-6} K kg^{-1} m^2 s^{-1}) at 0600 UTC

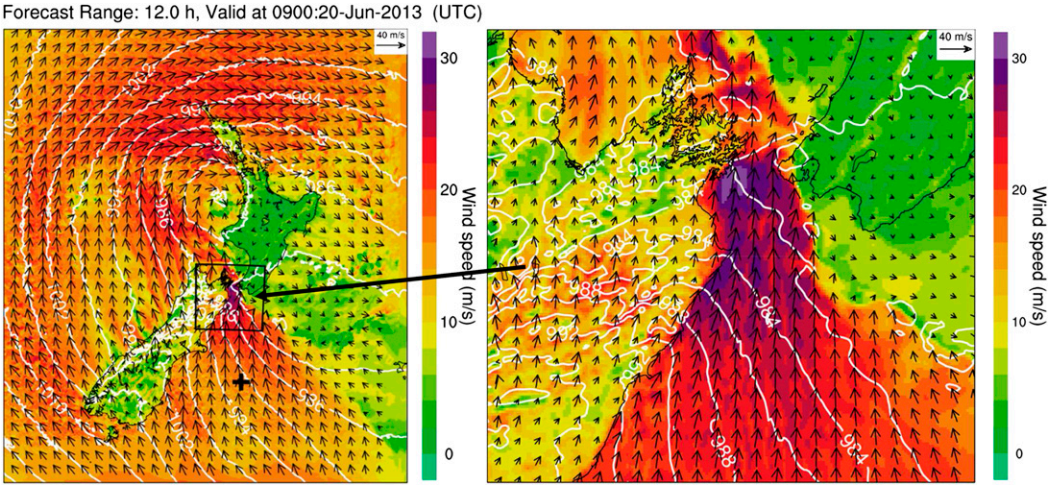

FIG. 3. Forecasted surface winds, mean sea level pressure (hPa, white contours), and wind speed (shading) by NZCSM. The strongest surface winds were over Cook Strait. (left) The plus sign ("+") denotes the location where the environmental mean wind profile was calculated.

16 June to approximately −10 PVU at 0600 UTC 20 June 2013 (Figs. 5c,d), implying that diabatic heating associated with the moist processes also contributed to the development of the low. For more information about the diabatic heating process for the development a midlatitude cyclone over the ocean, one may refer to Reed et al. (1993), Kuwano-Yoshida and Asuma (2008), and Fu et al. (2014).

In the late afternoon and evening, south-southeasterly winds in the southwestern portion of the Wellington Storm impinged on the coastal regions and mountains in the northeast of the South Island. This led to cold strong

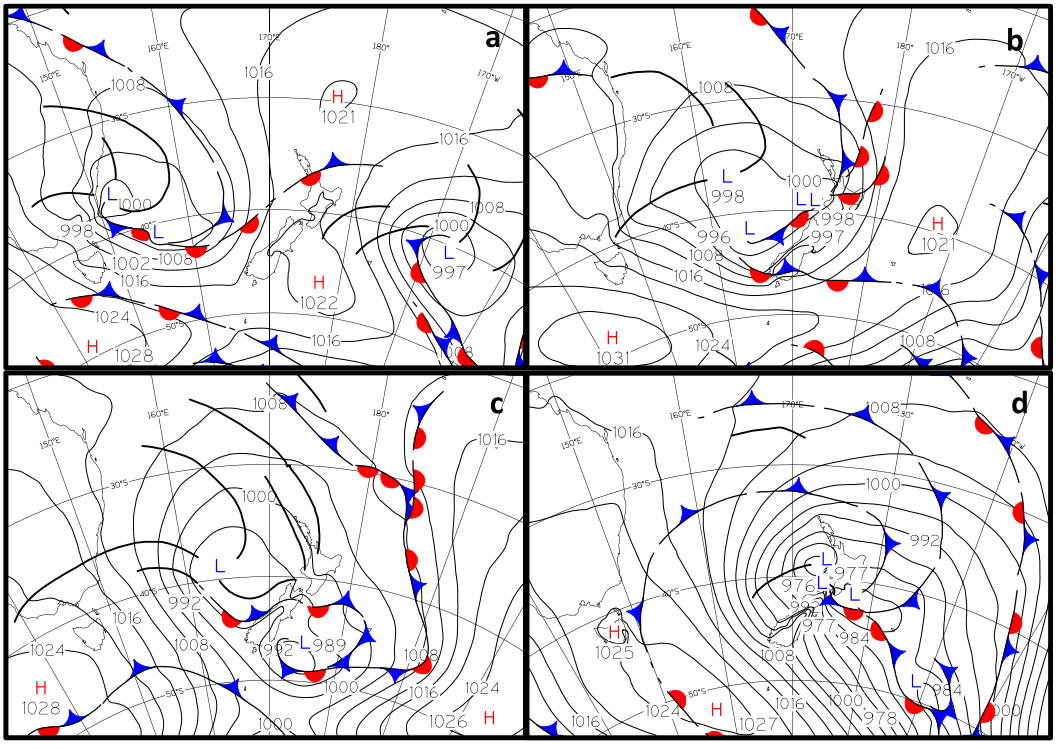

FIG. 4. Surface analysis for the Wellington Storm at (a) 0600 UTC 14 Jun, (b) 0600 UTC 16 Jun, (c) 0600 UTC 18 Jun, and (d) 0600 UTC 20 Jun 2013. (Courtesy of MetService New Zealand.)

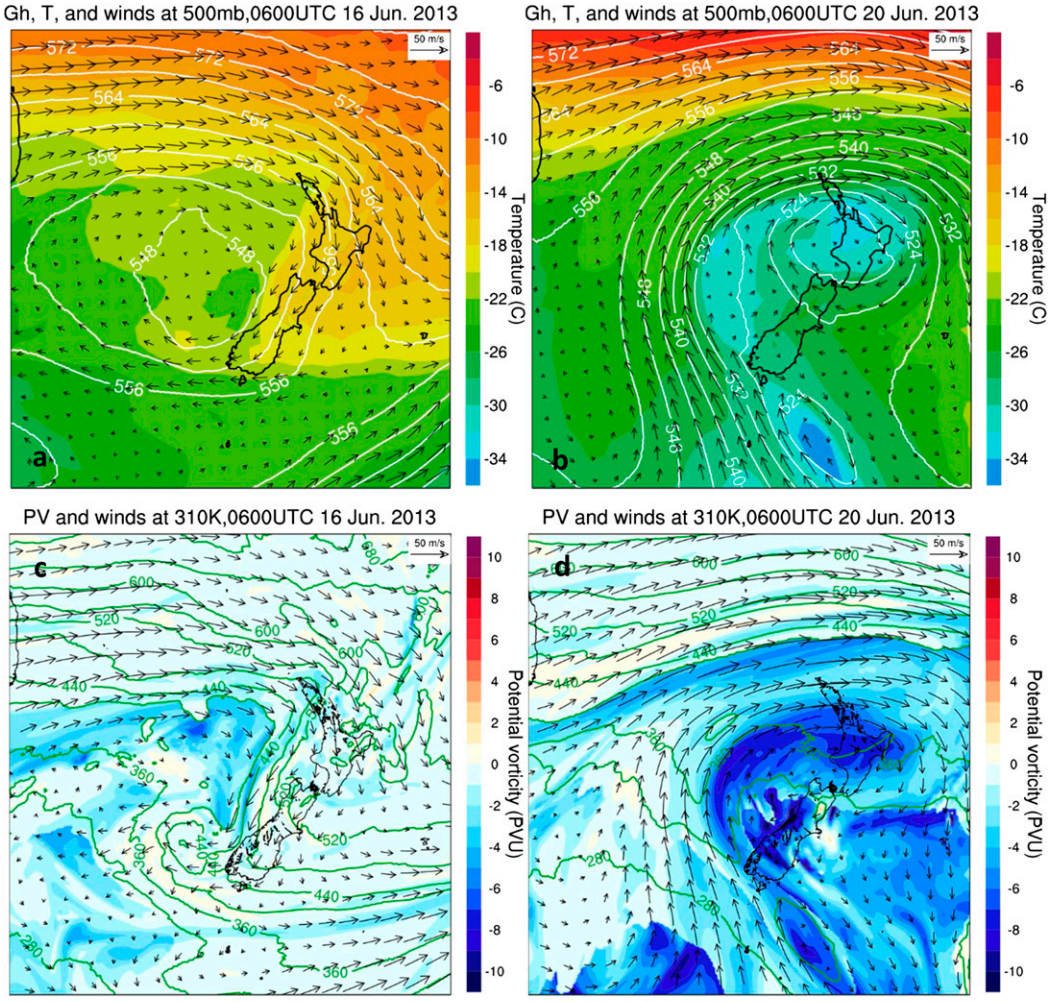

FIG. 5. Potential height (×10 m, white contours), winds, and air temperature at the 500-hPa level at (a) 0600 UTC 16 Jun and (b) 0600 UTC 20 Jun 2013. Pressure (hPa, green contours), winds, and Ertel potential vorticity $\{\mathrm{PV} = (\xi_\theta + f)[-g(\partial\vartheta/\partial p)]$, 1 PVU $= 10^{-6}\,\mathrm{K\,kg^{-1}\,m^2\,s^{-1}}\}$ on isentropic surface of 310 K at (c) 0600 UTC 16 Jun and (d) 0600 UTC 20 Jun 2013.

southerly winds (i.e., barrier jets) along the coast toward Cook Strait.

b. Model

In this study all of the numerical simulations were conducted using the NZCSM, a regional configuration of the Met Office Unified Model (MetUM; Webster et al. 2003; Davies et al. 2005). The NZCSM has a domain size (Fig. 3a) of 1200 (west–east) by 1350 (south–north) horizontal grid points with a horizontal grid spacing of ~1.5 km. It has 70 levels in the vertical up to 40 km above the mean sea level. The highest vertical resolution is in the lower boundary layer.

The NZLAM, also a local configuration of the MetUM (Webster et al. 2003; Yang et al. 2011, 2012), provided the initial conditions as well as lateral boundary conditions at 30-min intervals for NZCSM. NZLAM has a domain size of 324 × 324 grid points and ~12-km horizontal resolution. It has 70 levels in the vertical and the top level is at 80 km. A global configuration forecast run of the MetUM, initialized using a 4DVAR data assimilation scheme, provided the lateral boundary conditions for NZLAM. NZLAM is initialized four times a day (0000, 0600, 1200, and 1800 UTC) by using an incremental 3DVAR first guess at appropriate time (FGAT) analysis scheme (Lorenc et al. 2000).

The very high resolution of NZCSM resolves the mountains of New Zealand well. However, underestimations of mountain heights were found for mountains with half-widths of only a few kilometers. A typical example is Mt. Cook where the underestimation was ~900 m. As described later, Mt. Cook is far away

TABLE 1. A description of numerical experiments.

Expt name	Brief description
CTRL	Simulation without modifying the model terrain
TER0.0	Flat New Zealand land area with 0.1-m height
TER0.25	25% of the CTRL terrain height
TER0.5	50% of the CTRL terrain height
TER0.75	75% of the CTRL terrain height
TER1.1	110% of the CTRL terrain height
TER1.2	120% of the CTRL terrain height
TER1.3	130% of the CTRL terrain height
TER1.4	140% of the CTRL terrain height
TER1.5	150% of the CTRL terrain height
TER1.7	170% of the CTRL terrain height
TERmv	Moving the New Zealand terrain northward by 300 km
TERflatN	Flat North Island with 0.1 m above the mean sea level

from Cook Strait and has little effect on the winds there. For the major mountains in the northeast of the South Island, the underestimation of mountain heights was ~300 m or less, accounting for ~15% of the mountain heights or less. The effect of this underestimation on DSWs in Cook Strait will be discussed in the summary.

The NZCSM simulation was initialized at 2100 UTC 19 June 2013 from an NZLAM forecast initialized at 1800 UTC and run for 24 h for this study (called CTRL in Table 1). To investigate the effects of mountain heights on the DSWs, 10 more simulations with different model terrain heights were also conducted (Table 1). For TER0.0, all the land grid points were set 0.1 m above the mean sea level. For other experiments, the model terrain heights were set as a proportion of the CTRL terrain height. All the vegetation types and fraction were the same for all simulations. All NZCSM lateral boundaries are over the sea. These lateral boundary conditions were provided by NZLAM and kept the same for all experiments. The initial conditions of NZCSM over New Zealand were adjusted to accommodate the terrain heights for each experiment. A spinup of 2–4 h was allowed for in each experiment. In the following analyses we use output from NZCSM after the initial spinup time.

Figure 6 shows the simulated (CTRL) and observed wind speed at the three stations shown in Fig. 1b. At Cape Campbell and Wellington Airport, the observed strong winds from 0700 to 2000 UTC were well simulated by the model with relative errors (simulation errors/observations) of 2%–15%. These strong winds were actually the barrier jets that will be described later. At Brothers Island (Fig. 6c), the simulated strong wind speed occurred between 0900 and 2000 UTC 20 June, corresponding well to observations, but 10–15 m s^{-1} weaker than the observations. Brothers Island is ~250 m long and ~60 m wide and thus not resolved by NZCSM. Further, the wind observation site on Brothers Island is at 67 m above sea level with a steep cliff on the southern approach, while the simulated wind at the Brother Island is at sea level. This likely accounts for a large fraction of the magnitude of errors in wind speed but not their timing.

At the three stations, large errors (much weaker simulated winds) were found at 0500 and 0600 UTC (Fig. 6). Simulated strong southerlies occurred 2–3 h later than in the observations. During this time period, a cold front was observed to pass over these stations. Strong southerly winds and heavy rainfall occurred after the passage of the cold front. From rainfall observations and simulations (not shown), the simulated cold front passed each of the three stations about 2 h later than indicated by the observations. This is the main reason for the large errors in the simulated winds during this time period. Another possible reason is the error in the intensity of the simulated cold front in terms of the air temperature gradient across the front. Part of the reason for the slower movement of the simulated cold front will be discussed in the summary.

From 0900 to 1100 UTC 20 June, maximum hourly wind gusts were found at the three stations (Fig. 2) and the simulated wind speed was close to the observations (Fig. 6). This period also excluded the time period (0500–0800 UTC) when larger errors in simulated winds occurred associated with the passage of the cold front. Thus, in the following analysis, we will mainly analyze the model outputs during 0900–1100 UTC 20 June to understand the reasons for the occurrence of DSWs in Cook Strait.

c. *Parameters*

To understand the effects of the mountains of the South Island on the strong airflow associated with the Wellington Storm, parameters controlling the dynamics such as the Froude number ($F_m = U/Nh_m$), mountain Rossby deformation radius ($L_m = Nh_m/f$), and Burger number B need to be determined. For the Southern Alps, h_m = ~2250 m (Revell et al. 2002). However, airflow speed U and N need to be determined specifically. For this investigation, U and N should represent the upstream environmental airflow to the east of the South Island, which is not affected by the thermal and dynamical forcing of the mountains. To meet these conditions, we select an area occupied by 20 × 20 grid points of the NZCSM with its center located at −45°S, 176°E, about 200 km to the east of the central coast of the South Island (indicated in Fig. 3a) to avoid any possible effects of the mountains of New Zealand on the

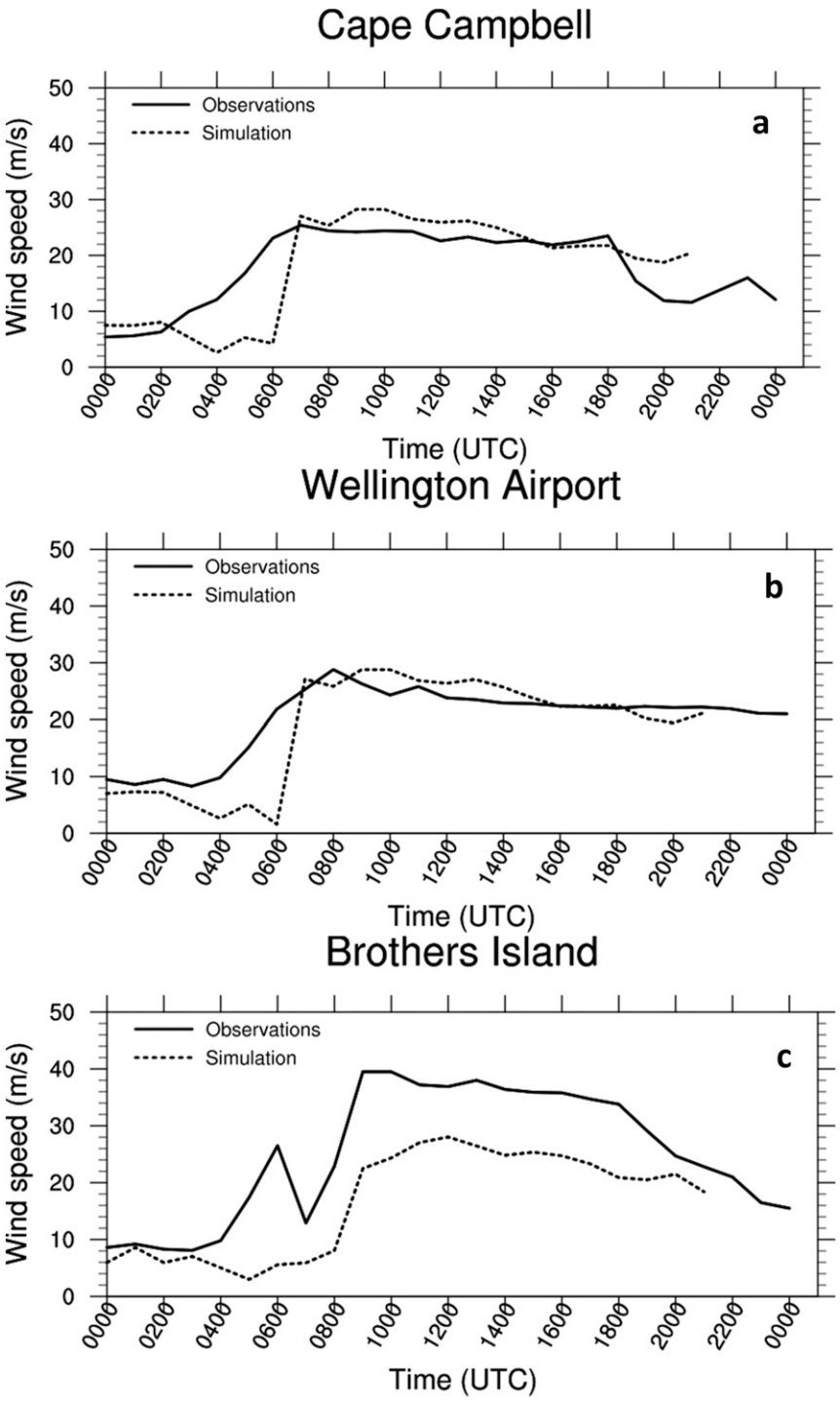

FIG. 6. Observed surface wind speed (solid lines) and simulated surface wind speed (dotted lines) on 20 Jun 2013 at (a) Cape Campbell, (b) Wellington Airport, and (c) Brothers Island.

environmental airflow. At each model level, the selected area mean values of U and N were calculated using model output from the CTRL run. Because we want to compare the results from our NZCSM experiments with the linear-scale analysis of Overland and Bond (1995) about the relationship of barrier jet strength with Froude number (F_m), the calculation of N here is from potential temperature (or dry atmosphere). Figure 7

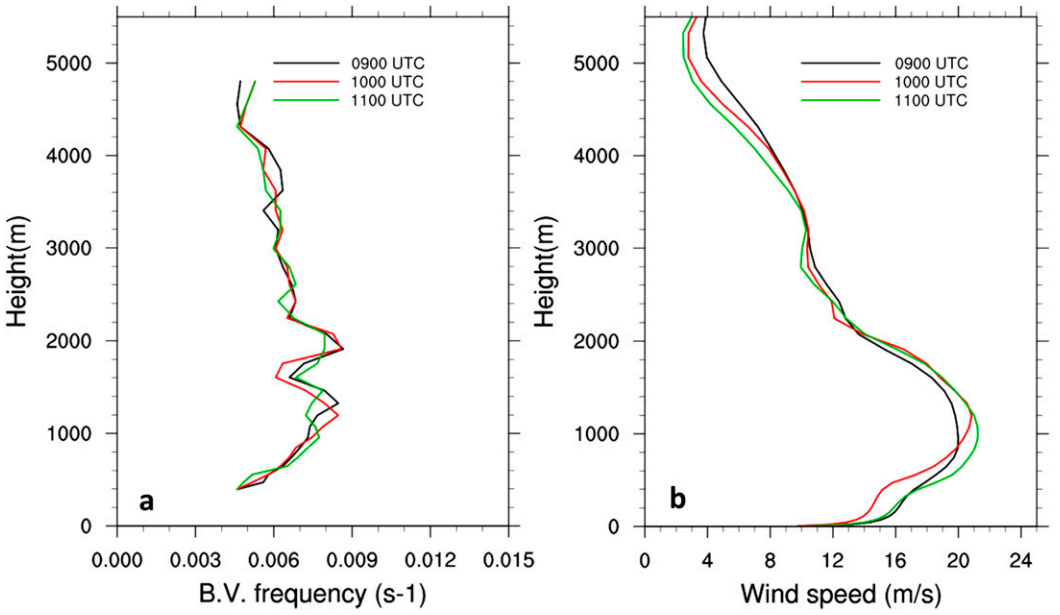

FIG. 7. (a) Vertical profiles of Brunt–Väisälä frequency N and (b) profiles of wind speed perpendicular to the South Island from a $30 \times 30\,km^2$ area around −45°S, 176°E (denoted by the "+" in the left panel of Fig. 3) using CTRL simulation.

shows the profiles of the environmental winds perpendicular to the South Island and N upstream of the South Island for 3 h where the strongest DSWs occurred in Cook Strait. Near the sea surface in the boundary layer, the effects of sea surface thermal forcing and boundary layer mixing led to very small N below 400 m. These are not shown in the profiles (Fig. 7a) and were ignored in the calculation of the mean value. From 400 to 1000 m, N increased with height, while from the ~1.8-km level and higher, it overall decreases with height. Large variations of N were found in the 1–1.8-km layer with two maxima ($\sim 0.009\,s^{-1}$) and a minimum ($\sim 0.006\,s^{-1}$). Because the effective mountain height is ~2.2 km, the average value of N was calculated only between 0.4 and 2.2 km to be $\sim 0.0075\,s^{-1}$. Although the N used in this study is dry N, please note that for this case study the profiles of the mean dry N from potential temperature (Fig. 7a) were very close to those of the mean moist N from virtual potential temperature below 5 km (not shown). Reinecke and Durran (2008) used two methods to estimate the low-level air stability, averaging N below the mountain crest and using the bulk change in potential temperature between the ground and the crest level. They indicated that one method is not always better than the other. The best method depends on the application. Here the method we used to calculate N is the "averaging" method used by Reinecke and Durran (2008). The impact of the uncertainty in the determination of N will be discussed in section 5.

A strong wind speed ($\sim 22\,m\,s^{-1}$) perpendicular to the South Island was found in the 1–1.5-km layer (Fig. 7b). Above the 1600-m level, wind speed decreased with height. Below 1000 m wind speed increased with height. The mean wind speed was $\sim 18.5\,m\,s^{-1}$ for the layer from 400 m to 2.2 km. The mean wind direction was ~150° for this layer. Therefore, $F_m = 1.1$. According to Overland and Bond (1995), for $f = 0.0001\,s^{-1}$ and $F_m > 1$ the mountain Rossby radius $L_m = \sim 170$ km for the Southern Alps. Based on this mountain Rossby radius value, the Southern Alps are too far from the Cook Strait region to influence the local airflow. Thus, under a southerly or southeasterly flow, the effect of major mountains on the winds in the Cook Strait would come from the nearby mountains in the northeast of the South Island. For the northeast mountains of the South Island, the greatest height in the model terrain is ~2000, 2000, or 1900 m may be a more suitable effective mountain height. Mountain half-width is ~40 km. This gives $B =$ 3.56 or 3.75 and $F_m = 1.23$ or 1.3 for $L = \sim 40$ km. These large B values imply that barrier jets could occur for the Wellington Storm due to the effects of the mountains in the northeast of the South Island.

3. Barrier jets

In this paper, following Li and Chen (1998) and others, barrier jets are defined to consist of two wind components. One is the environmental airflow parallel to the

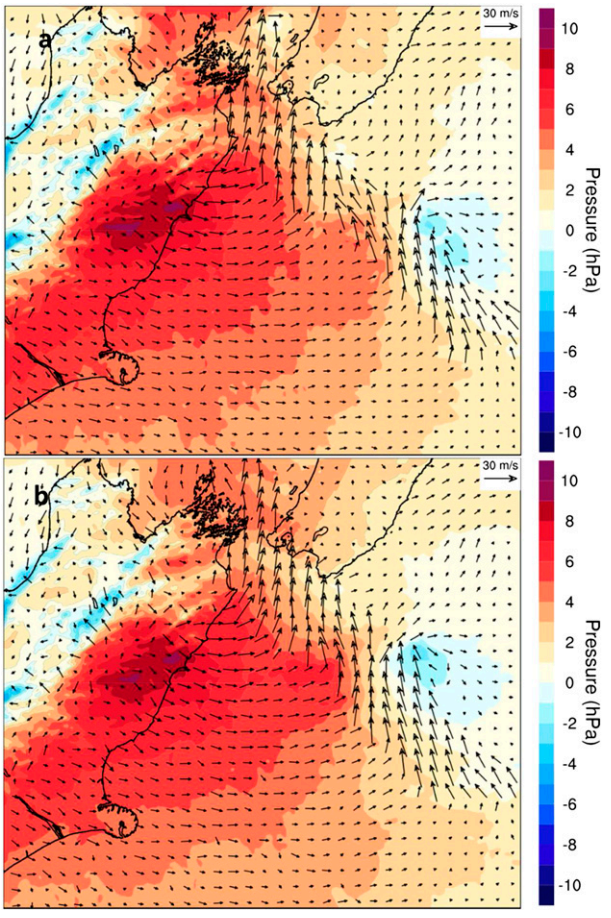

FIG. 8. The differences (CTRL − TER0.0) in winds and mean-sea level pressure (hPa) between the simulations by NZCSM with mountains (CTRL) and that without mountains (TER0.0) at (a) 1000 and (b) 1100 UTC 20 Jun 2013.

mountain ridges. The other is the ageostrophic wind resulting from local pressure gradients due to mountain effects. The best way to show the local pressure anomalies is to use the differences between the simulations with mountains and those without mountains.

Figure 8 shows the differences in the mean sea level pressure and surface winds between CTRL and TER0.0. When the south-southeasterly winds of the Wellington Storm impinged on the mountains in the northeast of the South Island (Fig. 3a), positive local pressure anomalies occurred (Fig. 8) due to adiabatic ascent of airflow as a result of orographic lifting. The maxima (8–10 hPa) were found over the windward coastal region. This is much higher than the maximum sea level pressure disturbance (~3 hPa) due to mountain blocking for normal weather conditions in the summer when the mean low-level wind speed was only about $\sim 5\,\mathrm{m\,s^{-1}}$ (Yang et al. 2011).

From the east coast of the South Island to Cook Strait, ageostrophic winds of 4–20 $\mathrm{m\,s^{-1}}$ were developed and strengthened by the local pressure gradient anomalies. The positive pressure anomalies gradually decreased offshore. Positive anomalies of pressure of about 1 hPa could still be found about 200 km to the east of the South Island. This indicates that the effects of the mountains of the South Island could extend about 200 km offshore, close to but longer than the mountain Rossby deformation radius (~170 km) calculated for the Wellington Storm in the last section. This is the reason that the mean wind profile and Brunt–Väisälä frequency were calculated for the environmental airflow about 200 km offshore as described earlier.

Along the northeast coastline, positive pressure anomalies can be found up to the 2000-m level and higher (Figs. 9a,b). Ageostrophic winds developed due to the pressure gradient anomalies and gradually strengthened along the cross section (alongshore). These ageostrophic winds combined with the environmental flow alongshore to form barrier jets with maximum wind speed ($\sim 38\,\mathrm{m\,s^{-1}}$) at the 600–800-m levels (Fig. 9b).

Figure 9c shows the wind speed parallel to the mountains along transect AB (Fig. 1b). Strong winds or barrier jets ($\sim 5\,\mathrm{m\,s^{-1}}$) were found over the coastline and gradually weakened offshore. Strong winds ($\sim 40\,\mathrm{m\,s^{-1}}$), even stronger than the barrier jets, were also found over the leeside mountains at the ~2-km level (Figs. 9c,d) as a result of the descent of airflow aloft over the leeside slopes for F_m slightly larger than 1. These strong winds were different from the barrier jets and did not impact on the Cook Strait region.

For the mountains over the northeast of the South Island, the aspect ratio (length/width) is greater than 2. As described in section 2, for the south-southeasterly flow associated with the Wellington Storm hitting these mountains, $F_m = 1.23 - 1.3$. According to Smith (1989), this implies a nonlinear mountain wave or wave breaking regime. The potential temperature contours (Fig. 9d) show pronounced wave patterns or gravity waves over the mountains below 4500 m.

4. Winds entering Cook Strait

The strong winds shown in Fig. 3 over Cook Strait have the appearance of gap winds. However, after further investigation, we suggest that this is not the case. The width of Cook Strait is not uniform and the smallest gap is around Brothers Island (Fig. 1b). According to the definition of gap winds (Pan and Smith 1999), the strongest winds occur at the exit of a gap. For this case, the strongest winds would occur to the north of Brothers Island (Fig. 1b). However, as shown in Fig. 3, the winds to the south of Brothers Island were slightly higher than those to the north. In addition, for gap winds, local

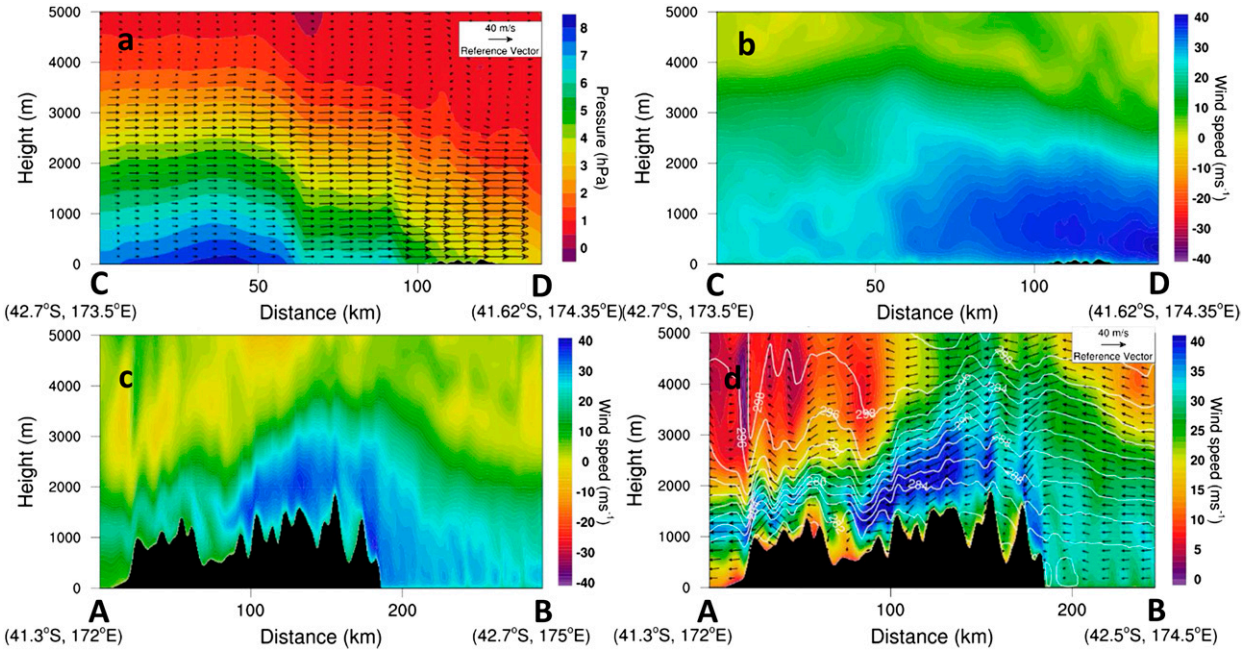

FIG. 9. (a) Cross section for line CD in Fig. 1b for the differences in winds alongshore and differences in pressure (shading) between CTRL and TER0.0 at 1000 UTC, and (b) for the alongshore wind component at 1000 UTC 20 Jun 2013. (c) Cross section for line AB in Fig. 1b for the alongshore wind speed (into the cross section) at 1000 UTC; and (d) wind vectors parallel to the cross section (across shore), potential temperature (contours), and horizontal wind speed (shading) at 1000 UTC 20 Jun 2013.

pressure immediately upstream of a gap is higher than that nearby the exit of the gap. As revealed in Fig. 8b, the local pressure at this time as a result of mountain effects upstream of Brothers Island (Fig. 1b) was lower than that to the north. A similar feature was also found for the sea level pressure (Fig. 10a). Further strong evidence comes from a numerical experiment conducted using the NZCSM in which the North Island was changed to a flat land surface only 0.1 m above sea level (TERflatN; Table 1), but the full South Island orography was kept. Cook Strait disappeared for this case. At 1100 UTC 20 June 2013 (Fig. 10), the wind speed maximum in Cook Strait for CTRL was only ~1 m s^{-1} larger than that of TERflatN. Overall, the simulated surface wind distributions/patterns in Cook Strait by TERflatN were very similar to those of CTRL. The wind speeds were also very close for the two simulations. The reason is very likely that for southerly winds prevailing in Cook Strait, the major

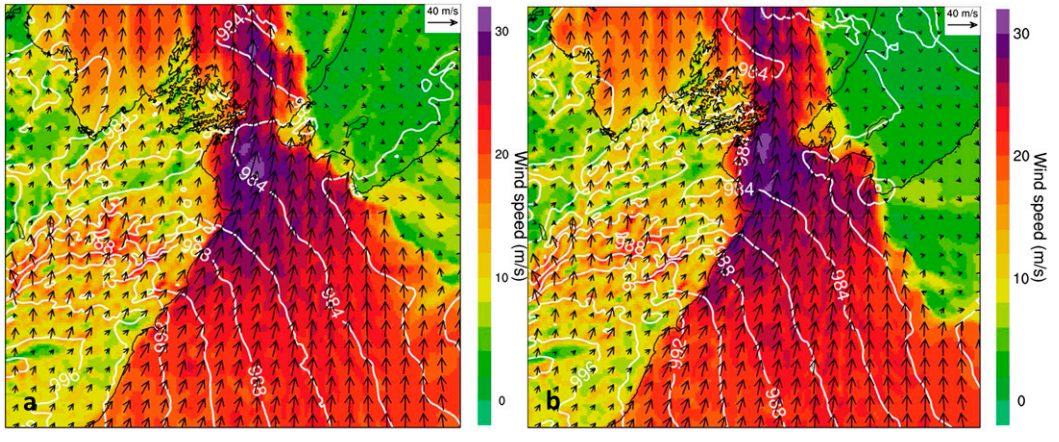

FIG. 10. Forecasted surface winds, mean sea level pressure (hPa, white contours), and wind speed (shading) by NZCSM at 1100 UTC 20 Jun 2013 for (a) CTRL and (b) TERflatN.

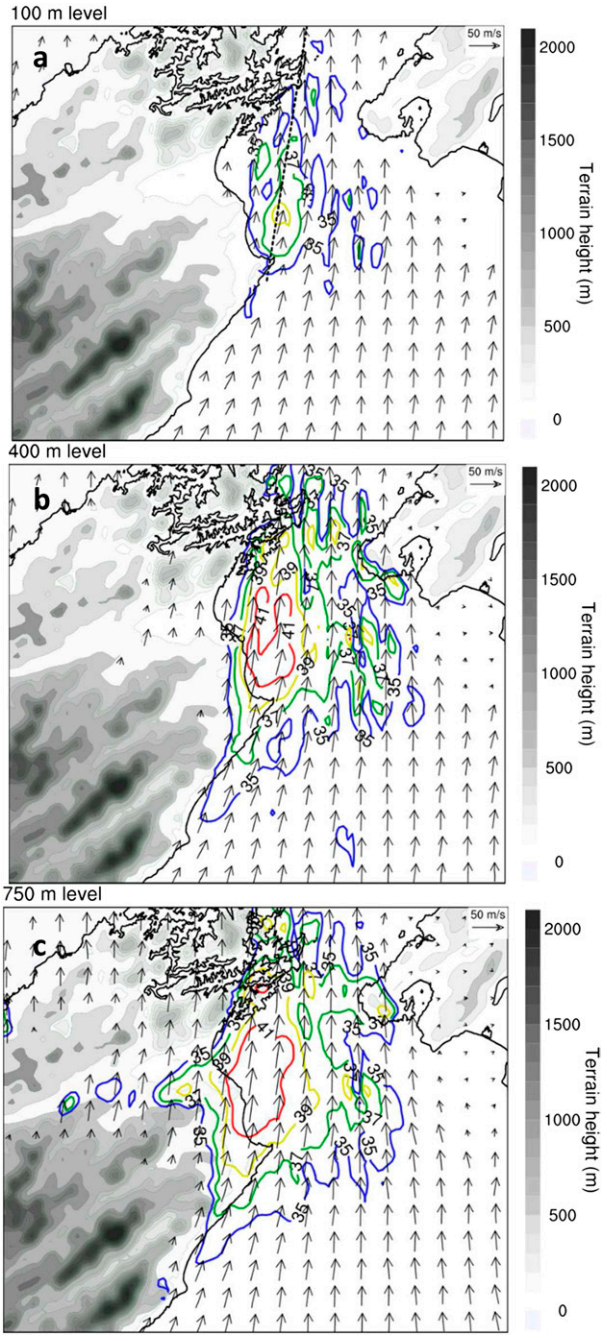

FIG. 11. Simulated wind vectors and wind speed at (a) 100, (b) 400, and (c) 750 m MSL at 1000 UTC 20 Jun 2013. Only contours of 35 (blue), 37 (green), 39 (yellow), and 41 m s^{-1} (red) were drawn. The dotted line in (a) coincides with line EF (Fig. 1b).

mountains of the North Island lie far away downstream or to the east and have little effect on Cook Strait. In addition, for this case, low-level southerly winds were mainly to the west of the North Island (Fig. 3).

Figure 11 shows the simulated horizontal wind speed and vectors at three levels. From 100 to 750 m, winds stronger than 39 m s^{-1} were mainly located over the western coastal region of Cook Strait. In contrast, the wind speed over the eastern coastal region of Cook Strait was 3–10 m s^{-1} weaker. This wind speed distribution in Cook Strait is consistent with observations. Brothers Island lies at the west edge of Cook Strait and Cape Campbell at the southernmost point of the west coast of Cook Strait. From 0600 to 1800 UTC 20 June when very strong winds occurred in Cook Strait, the hourly maximum gusty winds at Brothers Island was 8–16 m s^{-1} stronger than that at Wellington Airport on the eastern side (Fig. 2) of Cook Strait. Part of the difference was due to not resolving Brothers Island as discussed in section 2. The wind speed at Cape Campbell was 3–10 m s^{-1} stronger than at Wellington Airport. This also helps confirm the overall reliability of the NZCSM simulation for the Wellington Storm.

For the winds in Cook Strait from the surface to the ~400-m level, the orientation of the wind speed maximum area was roughly north to south, as denoted by the dotted line in Fig. 11a. The wind speed maximum was over the sea about 5–10 km off the west coast of Cook Strait. This suggested that the strong winds were not from the west coast of Cook Strait.

For the cross section EF (Fig. 2b) along Cook Strait, a pronounced local pressure gradient due to mountain blocking can be found below the 2-km level (Fig. 12a). From the southern end of the cross section to the middle, the pressure gradient increased the wind speed at low levels. In the northern portion of the cross section, the local pressure gradient slightly slowed the winds. This counter–wind pressure gradient in this area can also be found in Fig. 8b. Maximum wind speed (~42 m s^{-1}) was found at the 600–800-m level (Fig. 12b), almost the same height as the maximum barrier jets along the northern section of the east coast of the South Island (Fig. 9b), but the maximum wind speed was ~4 m s^{-1} stronger due to additional increase in wind speed by the local pressure gradient in the southern Cook Strait region as described earlier. These results suggested that the strong winds in Cook Strait were an extension of the barrier jets developed along the northern section of the east coast of the South Island.

5. Effects of mountain heights on barrier jets

Assuming uniform wind speed and static stability, inviscid and adiabatic conditions and using linear-scale analysis, Overland and Bond (1995) showed that the enhancement in the mountain parallel wind component is $\Delta V = U$ for $F_m < 1$ or $\Delta V = Nh_m$ for $F_m \geq 1$. In other words, for the $F_m < 1$ regime, barrier jet strength is fixed and independent of mountain height, where U is the

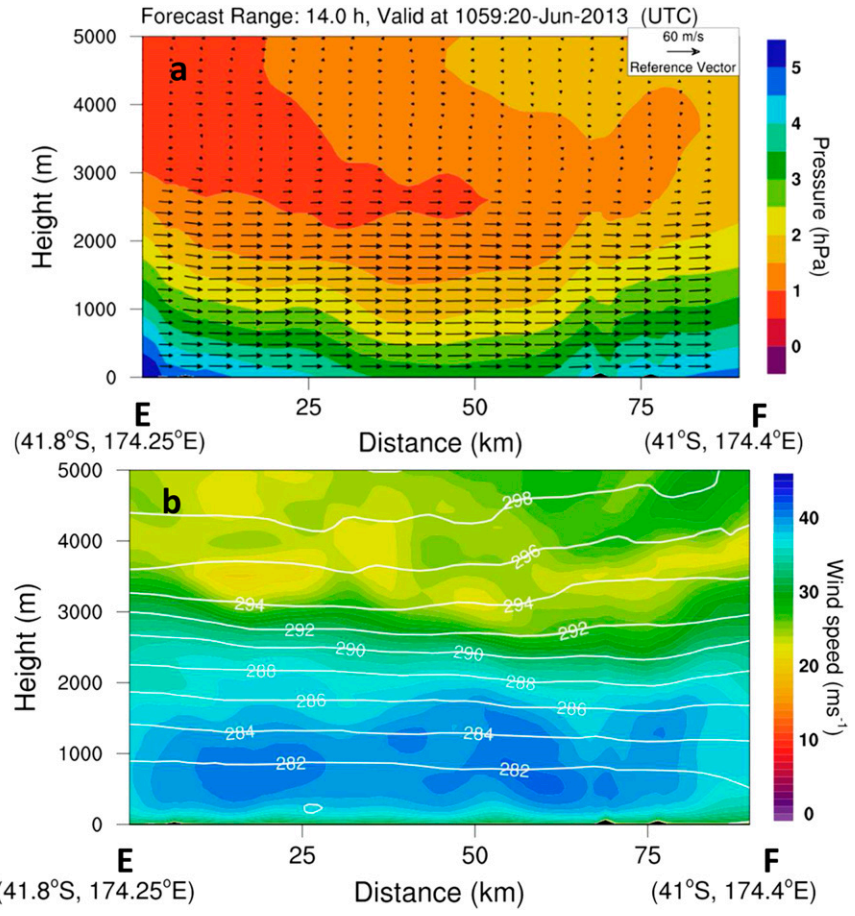

FIG. 12. (a) Cross section for line EF in Cook Strait (Fig. 1b) for the differences in winds along the cross section and differences in pressure (shading) between CTRL and TER0.0 at 1100 UTC; (b) for the horizontal wind speed and potential temperature at 1100 UTC 20 Jun 2013.

wind speed perpendicular to the mountain ridge. For the $F_m \geq 1$ regime for an airflow with fixed U and N, the barrier jet strength is determined by mountain height h_m. In this section we describe several numerical experiments with different scaled mountain heights (Table 1) to investigate the effects of mountain height on barrier jet strength including nonlinear effects and dynamical and thermal processes.

Figure 13 shows the simulated surface winds and sea level pressure for four different mountain heights at 1100 UTC 20 June. For TER0.0 with a flat surface of 0.1 m, strong southerly winds (environmental flow) were found to the east of the South Island and reached the southernmost point of Cook Strait (Fig. 13a). For TER0.25 (Fig. 13b), relatively strong southerly winds (barrier jets) reached farther into Cook Strait itself. As mountain height increased for experiment TER0.5 (Fig. 13c), strong southerly winds reached the middle region of Cook Strait. For experiment TER0.75, with a further increase in mountain height (Fig. 13d), strong southerly winds extended right through the Cook Strait region. For the CTRL run, with higher mountains than TER0.75, very strong winds extended even farther to the north (Figs. 3b and 10a). Figure 14 shows the wind component along the east coast of the South Island (line CD in Fig. 1b). Without mountains, the environmental airflow still had an alongshore wind component (Fig. 14a). This wind component is considered to be part of the barrier jet in this study. It is quite clear that the barrier jets strengthened with increasing mountain height. The depth of the barrier jets also increased with increasing mountain height.

Figure 15 shows the barrier jet strength for different mountain heights from the numerical experiments (Table 1) and the scale analysis (Overland and Bond 1995). The simulated barrier jet strength was determined by using the mean of the maximum wind speed (or the strongest barrier jets) at 0900, 1000, and 1100 UTC in the cross

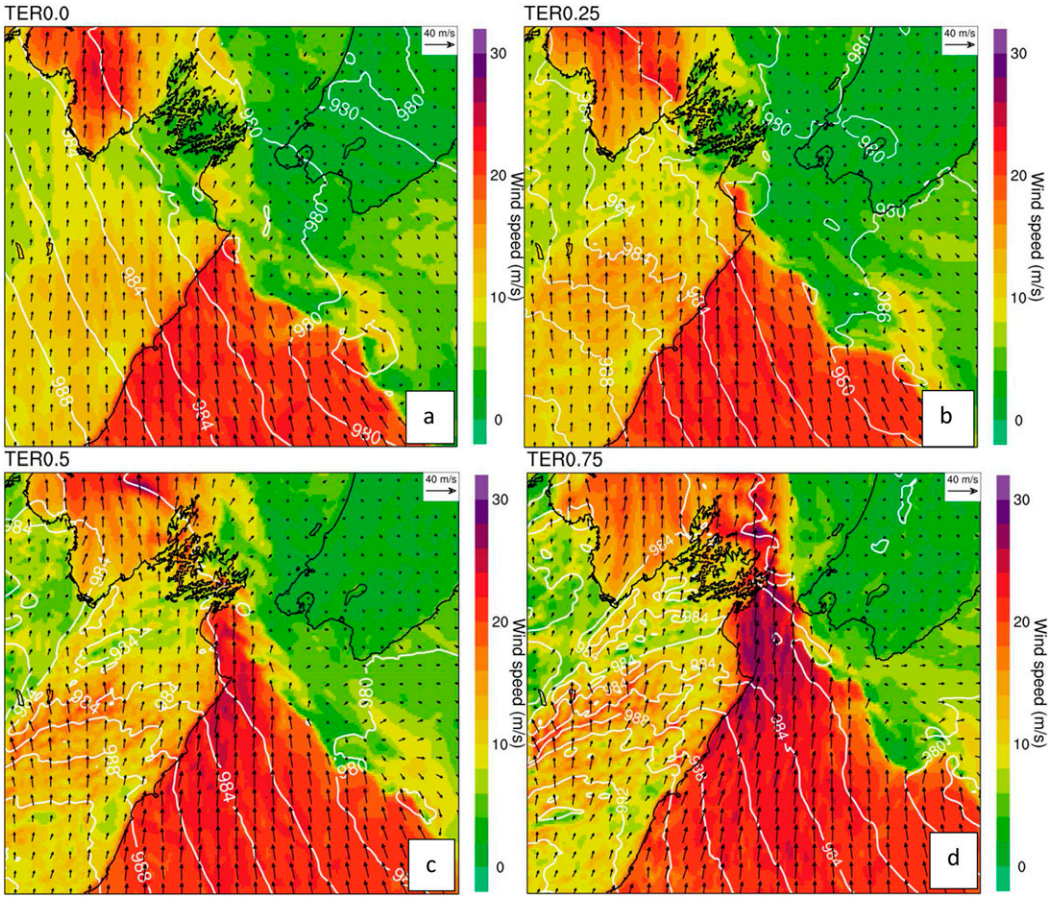

FIG. 13. As in Fig. 3 (the right panel), but for (a) TER0.0, (b) TER0.25, (c) TER0.5, and (d) TER0.75.

section parallel to the northeast mountains of the South Island (Fig. 14). The maximum wind speed in Fig. 14a (TER0.0) was added to ΔV from the scale analysis as described earlier, because the barrier jets also consisted of the environmental airflow parallel to the mountains in this study. According to Revell et al. (2002), the effective mountain height of the main spine of the Southern Alps is ~2250 m for a westerly airflow. For a southerly or south-southeasterly airflow hitting the northeast mountains of the South Island, the effective mountain height would be ~2000 or ~1900 m as described in section 2c. In Fig. 15, barrier jet strengths corresponding to all these three effective mountain heights were calculated from scale analysis. Three possible regimes are shown in the diagram based on Froude numbers.

For the $F_m > 1$ regime, the simulated barrier jets strengthen with increasing mountain heights, consistent with the scale analysis. But the variation is not so linear due to the nonlinear processes included in the simulation. For the $F_m < 1$ regime, the simulated barrier jets were still strengthened with increasing mountain heights, but the strengthening rate was very small, about 0.4–0.5 m s^{-1} $(0.1H)^{-1}$. In contrast, for the $F_m > 1$ regime, the strengthening rate was 1.5–1.8 m s^{-1} $(0.1H)^{-1}$. The effect of mountain height on the strength of the simulated barrier jet was different between the $F_m > 1$ regime and the $F_m < 1$ regime, consistent with the scale analysis. However, the strengthening of the simulated barrier jets with increasing mountain heights for the $F_m < 1$ regime is different from the scale analysis (i.e., consistent wind speed).

For the model simulation, the possible range of the effective mountain heights is 2250–1900 m for airflow affecting the northeast of the South Island as discussed earlier. This is equivalent to mountain height from $1.1H$ to $1.3H$ corresponding to $F_m = 1$ or very close to 1 (Fig. 15). From TER1.1 ($1.1H$) to TER1.2 ($1.2H$), the barrier jet strength was almost the same. However, a large increase was found for the jet strength from TER1.2 to TER1.3. Large variations of the barrier jet strength may occur for F_m very close to 1. This is different from the linear-scale analysis.

Figure 15 was plotted using the "averaging" method to calculate Brunt–Väisälä frequency. Using the Bulk

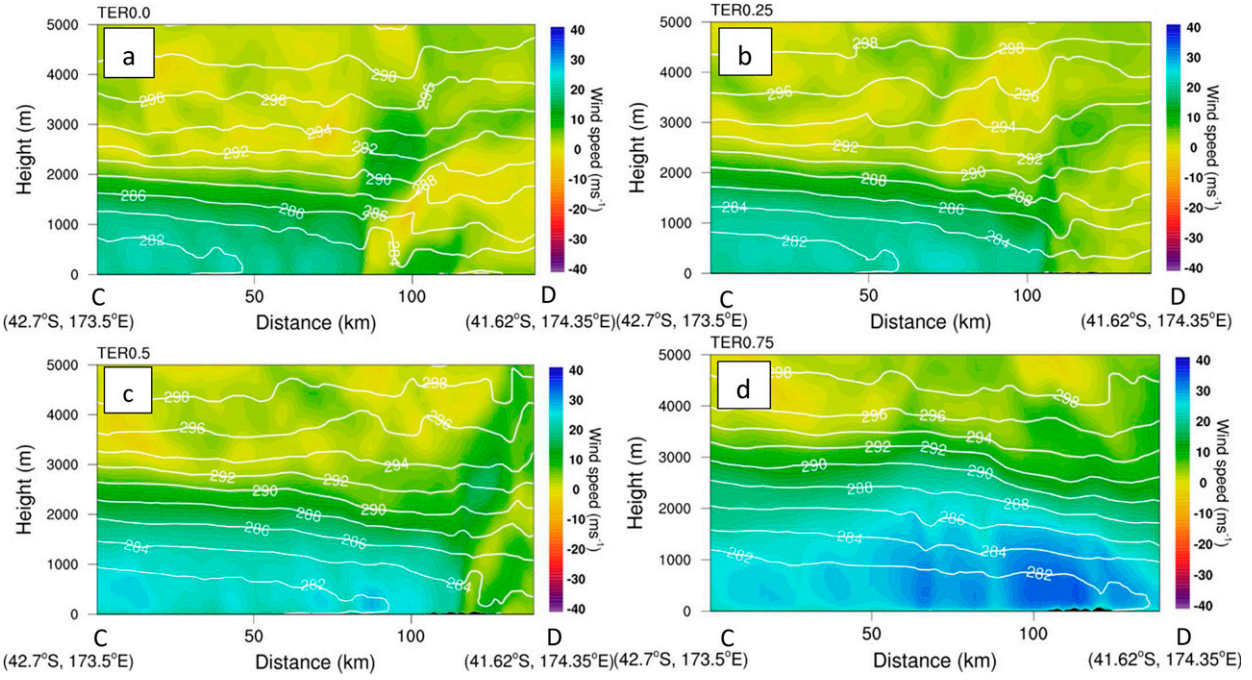

FIG. 14. Cross section of alongshore wind component and potential temperature for line CD in Fig. 1b for (a) TER0.0, (b) TER0.25, (c) TER0.5, and (d) TER0.75.

method (Reinecke and Durran 2008), the frequency was $\sim 0.0095\,s^{-1}$, slightly higher than the averaging method. This will make the maximum wind speed from the linear-scale analysis about $4\,m\,s^{-1}$ stronger, and a slight left shift of the F_m very close to 1 regime (gray area).

6. Effects of airflow directions on barrier jets

Assuming an incoming environmental airflow with speed V at an angle α ($<90°$) to a mountain ridge, then the wind components parallel to and perpendicular to the mountain ridge are $V\cos\alpha$ and $V\sin\alpha$, respectively. Based on the linear-scale analysis of Overland and Bond (1995), for the $F_m \le 1$, the enhancement in the wind component parallel to the mountain ridge is $V\sin\alpha$. Then the wind speed of the barrier jet as defined in this paper as $V\cos\alpha + V\sin\alpha$ (assuming linear processes). The maximum strength of the barrier jet is thus attained when $\tan\alpha = 1$ or $\alpha = 45°$. For $F_m > 1$, the enhancement in the wind component parallel to the mountain ridge is

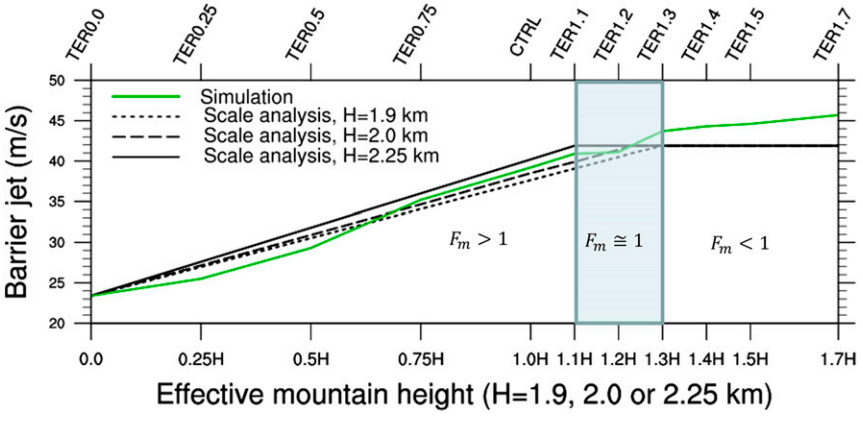

FIG. 15. The relationship of barrier jet strength and effective mountain heights from simulations and scale analysis (Overland and Bond 1995). The shading was possible $F_m = 1$ or very close to 1 regime. The lower axis shows the effective mountain height for each experiment and the upper axis shows each of the experiments (Table 1) corresponding to the mountain height.

TABLE 2. The mean low-level (400–2200 m) incoming wind speed and direction with respect to the orientation of the mountain ridges in the northeast of the South Island and the corresponding maximum barrier jets at various times (UTC) on 20 Jun 2013.

Time (UTC)	0900	1000	1100	1800	1900	2000
Max barrier jet ($m\,s^{-1}$)	39.0	40.2	39.0	34.0	32.7	31.1
Mean incoming wind ($m\,s^{-1}$)	21.0	20.0	20.0	22.0	21.9	22.0
Incoming wind direction	49°	52°	49°	57°	57°	58°

$Nh_m = V\sin\alpha/F_m$. Assuming constant F_m, then the wind speed of the barrier jet is $V\cos\alpha + (V\sin\alpha/F_m)$. To reach the maximum strength of the barrier jet, one requires $\tan\alpha = 1/F_m$. For $F_m = 1.23$ to 1.3 as described in section 2c for airflow hitting the mountains in the northeast of the South Island, α is 38°–40°. Thus, even if the airflow speed and Froude number are the same, the barrier jet strength is sensitive to the airflow direction.

The DSWs in Cook Strait were due to the southerly or south-southeasterly winds in the southwestern area of the Wellington Storm hitting the mountains in the northeast of the South Island. With the southeasterly movement of this storm, the wind direction of the airflow with respect to the orientation of the South Island may change. This may result in variation of the barrier jet strength. To show this variation, we selected an area of 20 × 20 grid points of NZCSM with its center located at −45°S, 176°E (denoted by a plus sign"+" in Fig. 3a). The average u and v components of the simulated winds for this area at model levels from 400 to 2200 m were calculated for the CTRL experiment. Then the mean wind speed and wind direction relative to the orientation of the South Island were calculated and are shown in Table 2. At 0900, 1000, and 1100 UTC 20 June, the mean of the incoming wind speed was 20–21 $m\,s^{-1}$ and the wind direction was 49°–52° relative to the orientation of the South Island. The barrier jet was 39.0–40.2 $m\,s^{-1}$ along the northeastern coast of the South Island. At 1800, 1900, and 2000 UTC 20 June, the average incoming wind speed was ~22 $m\,s^{-1}$ and the direction was 57°–58°, while the barrier jet flow weakened to 31.1–34 $m\,s^{-1}$. It is interesting to note that when the direction of the incoming airflow ($F_m = 1.23 - 1.3$ as described earlier) was closer to 38°–40° earlier on 20 June, the barrier jets were stronger for almost the same incoming wind speed.

To further investigate the influence of incoming wind direction on the barrier jets, we conducted another experiment by moving the New Zealand terrain 300 km to the north. This is equivalent to a 300-km southward displacement of the Wellington Storm. Because the lateral boundaries of NZCSM are over the sea, moving the terrain inside the model domain does not change the lateral boundary conditions. With this change, the airflow in the Wellington Storm hitting the South Island changed to south-southwesterly from south-southeasterly in CTRL. The simulated surface winds and sea level pressure at two times are shown in Fig. 16. Relatively strong winds reached the middle southeastern coast of the South Island at 1100 UTC 20 June (Fig. 16a), and reached Cook Strait 3 h later (Fig. 16b). At this time, the wind strength in the Cook Strait was much weaker than that of CTRL (Fig. 3). This further supports the idea that the incoming wind direction affects barrier jet strength.

These analyses indicate that for a storm affecting New Zealand, the strength of barrier jets and southerly winds developing in the Cook Strait region is sensitive to the precise location of the storm center. This helps explain that while storms affecting New Zealand with almost the same intensity (in terms of central surface pressure) as the Wellington Storm are not uncommon, the winds

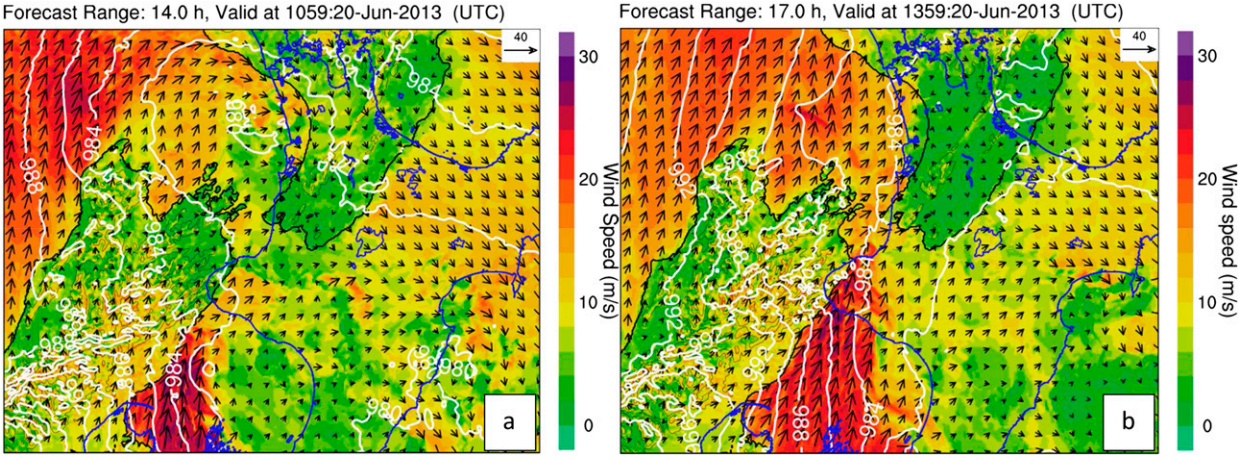

FIG. 16. As in Fig. 3 (the right panel), but for TERmv at (a) 1100 and (b) 1400 UTC 20 Jun 2013. The black lines denote the coastlines of the moved islands. The blue lines denote the real coastlines.

experienced in the Cook Strait region during the Wellington Storm are not that common.

7. Summary

Damaging southerly winds, associated with the Wellington Storm, occurred in the Cook Strait and coastal Wellington region during the night of 20 June 2013, causing severe damage to property and infrastructure. The DSWs in the Cook Strait region were stronger than elsewhere in the storm. Storms with the same minimum sea level pressure as the Wellington Storm (~976 hPa) are not unusual; however, the occurrence of the DSWs was unusual. Numerical experiments and simulations using the NZCSM have been conducted to investigate the reasons.

Analyses showed that the DSWs in Cook Strait associated with the Wellington Storm were actually barrier jets that developed along the northern section of the east coast of the South Island. When the strong south-southeasterly winds in the Wellington Storm impinged on the northeast mountains of the South Island, local pressure anomalies and local pressure gradients were generated. This led to the development of ageostrophic winds. These alongshore ageostrophic winds combined with the mean environmental airflow component parallel to the mountain ranges to form the barrier jets (i.e., strong low-level winds that moved north-eastward approximately parallel to the east coast of the South Island and entered Cook Strait). After the barrier jets entered Cook Strait, the wind speed was further increased by $\sim 4\,\mathrm{m\,s^{-1}}$ due to the local pressure gradients generated in the southern Cook Strait from mountain blocking.

Based on Overland and Bond (1995), assuming uniform airflow and static stability, inviscid and adiabatic conditions, the strongest barrier jet is reached for the $F_m \leq 1$ regime when the direction of the incoming airflow is 45° with respect to the orientation of the mountain range. For the $F_m > 1$ regime, the strongest barrier jet is reached when the airflow direction is $\tan^{-1}(1/F_m)$ (<45°). The effect of the incoming airflow direction on barrier jet strength is supported by our numerical experiments. These analyses indicate that for a storm affecting New Zealand, the strength of barrier jets and southerly winds developing in the Cook Strait region is sensitive to the precise location of the storm center. This helps explain that while storms affecting New Zealand with almost the same intensity (in terms of central pressure) as the Wellington Storm are not uncommon, the winds experienced in the Cook Strait region during the Wellington Storm are not that common.

Numerical experiments that used scaled New Zealand orography showed that barrier jets along the northern section of the east coast of the South Island are affected by the mountain heights. For the $F_m > 1$ regime, the barrier jets became stronger and deeper with increasing mountain heights. This is consistent with the linear-scale analysis results of Overland and Bond (1995). The rate of strengthening is about $1.5\,\mathrm{m\,s^{-1}}$ for each 200-m increase in the mountain height up to 2000 m. For the $F_m < 1$ regime, the simulated barrier jets still strengthened with increasing mountain heights but at about $0.5\,\mathrm{m\,s^{-1}}$ for each 200-m increase of the mountain height, much smaller than for the $F_m > 1$ regime. The effect of mountain height on the simulated barrier jets was different for the $F_m > 1$ and the $F_m < 1$ regimes. This is also consistent with the linear-scale analysis. However, the slight strengthening of the barrier jets with an increasing mountain height for the $F_m < 1$ regime is different from the linear-scale analysis (i.e., consistent barrier jet strength). In addition, pronounced variations were found in the strength of the simulated barrier jets with different mountain heights for F_m very close to 1. This is also different from the linear-scale analysis. The results of these numerical experiments imply that numerical simulations using a lower topography than actual (usually the case in NWP forecasting) may lead to errors in timing and in forecasting the strength and direction of the damaging winds associated with barrier jets.

NZCSM underestimated the major mountain tops in the northeast of the South Island by ~300 m or less. This is equivalent to ~15% of the mountain height. The actual mountain heights are probably equal to those by increasing NZCSM mountain heights by 15%–20%. This is almost equivalent to TER1.2. In Fig. 15, the differences in wind speed of barrier jets between CTRL and TER1.2 was $\sim 3\,\mathrm{m\,s^{-1}}$. Thus, underestimation of mountain heights in the northeast of the South Island by NZCSM probably would lead to weaker simulated southerly winds in Cook Strait by $\sim 3\,\mathrm{m\,s^{-1}}$. In front of the southerly winds in Cook Strait was the cold front. This partly explains why the cold front moved more slowly than observations as described in section 2b. This process may also explain why the front moves faster in CTRL than in TER0.0, as visible in Fig. 8 showing the northwest–southeast-oriented band of strong wind speeds in the difference field.

Analysis of PV at isentropic surface implied that latent heat release associated with the moist processes contributed to the development of Wellington Storm. How did the moist processes affect the DSWs in the Cook Strait? The strong barrier jets entering the Cook Strait were caused by south-southeasterly environmental flow impinging on the mountains in the northeast of the South Island. This environmental flow is associated with the storm winds located in the southwest portion of

the storm. Moist processes probably strengthened the storm flow (or environmental flow), leading to stronger barrier jets and stronger DSWs in Cook Strait. On the other hand, ascent of airflow due to mountain blocking caused adiabatic cooling on the windward side of the mountains in the northeast of the South Island. Latent heat release from precipitation associated with the ascent of airflow on the windward side may partly balance the adiabatic cooling, leading to weaker barrier jets. Answering which of these effects dominates is left for a future investigation.

Acknowledgments. This research was carried out under research collaboration SC0128 with the Met Office and funded by NIWA under its Hazards Research Programme (2013/14 and 2014/15 SCI). The authors wish to acknowledge the contribution of NeSI to the results of this research and to thank the three anonymous reviewers for their constructive comments. New Zealand's national compute and analytics services and team are supported by the New Zealand eScience Infrastructure (NeSI) and funded jointly by NeSI's collaborator institutions and through the Ministry of Business, Innovation and Employment (http://www.nesi.org.nz).

REFERENCES

Bell, G. D., and L. F. Bosart, 1988: Appalachian cold-air damming. *Mon. Wea. Rev.*, **116**, 137–161, doi:10.1175/1520-0493(1988)116<0137:ACAD>2.0.CO;2.

Bousquet, O., and B. F. Smull, 2003a: Airflow and precipitation fields within deep Alpine valleys observed by airborne Doppler radar. *J. Appl. Meteor.*, **42**, 1497–1513, doi:10.1175/1520-0450(2003)042<1497:AAPFWD>2.0.CO;2.

——, and ——, 2003b: Observations and impacts of upstream blocking during a widespread orographic precipitation event. *Quart. J. Roy. Meteor. Soc.*, **129**, 391–409, doi:10.1256/qj.02.49.

Clark, T. L., and W. R. Peltier, 1984: Critical level reflection and the resonant growth of nonlinear mountain waves. *J. Atmos. Sci.*, **41**, 3122–3134, doi:10.1175/1520-0469(1984)041<3122:CLRATR>2.0.CO;2.

Colle, B. A., and C. F. Mass, 1995: The structure and evolution of cold surges east of the Rocky Mountains. *Mon. Wea. Rev.*, **123**, 2577–2610, doi:10.1175/1520-0493(1995)123<2577:TSAEOC>2.0.CO;2.

Davies, T., M. J. P. Cullen, A. J. Malcolm, M. H. Mawson, A. Staniforth, A. A. White, and N. Wood, 2005: A new dynamical core for the Met Office's global and regional modelling of the atmosphere. *Quart. J. Roy. Meteor. Soc.*, **131**, 1759–1782, doi:10.1256/qj.04.101.

Durran, D. R., 2003: Downslope winds. *Encyclopedia of Atmospheric Sciences*, J. A. Curry and J. A. Pyle, Eds., Elsevier Science Ltd., 644–650.

Fu, S., J. Sun, and J. Sun, 2014: Accelerating two-stage explosive development of an extratropical cyclone over the northwestern Pacific Ocean: A piecewise potential vorticity diagnosis. *Tellus*, **66A**, 23210, doi:10.3402/tellusa.v66.23210.

Kuwano-Yoshida, A., and Y. Asuma, 2008: Numerical study of explosively developing extratropical cyclones in the northwestern Pacific region. *Mon. Wea. Rev.*, **136**, 712–740, doi:10.1175/2007MWR2111.1.

Li, J., and Y.-L. Chen, 1998: Barrier jets during TAMEX. *Mon. Wea. Rev.*, **126**, 959–971, doi:10.1175/1520-0493(1998)126<0959:BJDT>2.0.CO;2.

Lilly, D. K., 1978: A severe downslope windstorm and aircraft turbulence event induced by a mountain wave. *J. Atmos. Sci.*, **35**, 59–77, doi:10.1175/1520-0469(1978)035<0059:ASDWAA>2.0.CO;2.

Lorenc, A. C., and Coauthors, 2000: The Met Office global three-dimensional variational data assimilation scheme. *Quart. J. Roy. Meteor. Soc.*, **126**, 2991–3012, doi:10.1002/qj.49712657002.

Marwitz, J. D., 1983: The kinematics of orographic airflow during Sierra storms. *J. Atmos. Sci.*, **40**, 1218–1227, doi:10.1175/1520-0469(1983)040<1218:TKOOAD>2.0.CO;2.

Mass, C. F., and G. K. Ferber, 1990: Surface pressure perturbations produced by an isolated mesoscale topographic barrier. Part I: General characteristics and dynamics. *Mon. Wea. Rev.*, **118**, 2579–2596, doi:10.1175/1520-0493(1990)118<2579:SPPPBA>2.0.CO;2.

Neiman, P. J., L. J. Schick, F. M. Ralph, M. Hughes, and G. A. Wick, 2011: Flooding in western Washington: The connection to atmospheric rivers. *J. Hydrometeor.*, **12**, 1337–1358, doi:10.1175/2011JHM1358.1.

Olson, J., B. A. Colle, N. A. Bond, and N. Winstead, 2007: A comparison of two coastal barrier jet events along the southeast Alaskan coast during the SARJET field experiment. *Mon. Wea. Rev.*, **135**, 3642–3663, doi:10.1175/MWR3448.E1.

Overland, J. E., and N. A. Bond, 1993: The influence of coastal topography: The Yakutat storm. *Mon. Wea. Rev.*, **121**, 1388–1397, doi:10.1175/1520-0493(1993)121<1388:TIOCOT>2.0.CO;2.

——, and ——, 1995: Observations and scale analysis of coastal wind jet. *Mon. Wea. Rev.*, **123**, 2934–2941, doi:10.1175/1520-0493(1995)123<2934:OASAOC>2.0.CO;2.

Pan, F., and R. B. Smith, 1999: Gap winds and wakes: SAR observations and numerical simulations. *J. Atmos. Sci.*, **56**, 905–923, doi:10.1175/1520-0469(1999)056<0905:GWAWSO>2.0.CO;2.

Parish, T. R., 1982: Barrier winds along the Sierra Nevada Mountains. *J. Appl. Meteor.*, **21**, 925–930, doi:10.1175/1520-0450(1982)021<0925:BWATSN>2.0.CO;2.

Pierrehumbert, R. T., and B. Wyman, 1985: Upstream effect of mountains. *J. Atmos. Sci.*, **42**, 977–1003, doi:10.1175/1520-0469(1985)042<0977:UEOMM>2.0.CO;2.

Reed, R. J., G. Grell, and Y.-H. Kuo, 1993: The ERICA IOP 5 storm. Part II: Sensitivity tests and further diagnosis based on model output. *Mon. Wea. Rev.*, **121**, 1595–1612, doi:10.1175/1520-0493(1993)121<1595:TEISPI>2.0.CO;2.

Reid, S., 1996: Pressure gradients and winds in Cook Strait. *Wea. Forecasting*, **11**, 476–488, doi:10.1175/1520-0434(1996)011<0476:PGAWIC>2.0.CO;2.

Reinecke, P. A., and D. R. Durran, 2008: Estimating topographic blocking using a Froude number when the static stability is nonuniform. *J. Atmos. Sci.*, **65**, 1035–1048, doi:10.1175/2007JAS2100.1.

Revell, M. J., J. H. Copeland, H. R. Larsen, and D. S. Wratt, 2002: Barrier jets around the Southern Alps of New Zealand and their potential to enhance alpine rainfall. *Atmos. Res.*, **61**, 277–298, doi:10.1016/S0169-8095(01)00142-9.

Richwien, B. A., 1980: The damming effect of the southern Appalachians. *Natl. Wea. Dig.*, **5**, 2–12.

Schwerdtfeger, W., 1975: Mountain barrier effect of the flow of stable air north of the Brooks Range. *24th Conf. on Climate of the Arctic*, Fairbanks, AK, 204–208.

Scinocca, J. F., and W. R. Peltier, 1993: The instability of Long's stationary solution and the evolution toward severe downslope windstorm flow. Part I: Nested grid numerical

simulations. *J. Atmos. Sci.*, **50**, 2245–2263, doi:10.1175/1520-0469(1993)050<2245:TIOLSS>2.0.CO;2.

Smith, R. B., 1985: On severe downslope winds. *J. Atmos. Sci.*, **42**, 2597–2603, doi:10.1175/1520-0469(1985)042<2597:OSDW>2.0.CO;2.

——, 1989: Hydrostatic airflow over mountains. *Advances in Geophysics*, Vol. 31, Academic Press, 1–41, doi:10.1016/S0065-2687(08)60052-7.

Webster, S., A. R. Brown, C. P. Jones, and D. R. Cameron, 2003: Improvements to the representation of orography in the Met Office Unified Model. *Quart. J. Roy. Meteor. Soc.*, **129**, 1989–2010, doi:10.1256/qj.02.133.

Yang, Y., M. Uddstrom, M. Revell, P. Andrews, H. Oliver, R. Turner, and T. Carey-Smith, 2011: Numerical simulations of effects of soil moisture and modification by mountains over New Zealand in summer. *Mon. Wea. Rev.*, **139**, 494–510, doi:10.1175/2010MWR3324.1.

——, ——, ——, ——, and R. Turner, 2012: Amplification of the impact of assimilating ATOVS radiances on simulated surface air temperatures over Canterbury by the Southern Alps, New Zealand. *Mon. Wea. Rev.*, **140**, 1367–1384, doi:10.1175/MWR-D-11-00185.1.

Yeh, H.-C., and Y.-L. Chen, 2003: Numerical simulations of the barrier jet over northwestern Taiwan during the mei-yu season. *Mon. Wea. Rev.*, **131**, 1396–1407, doi:10.1175/1520-0493(2003)131<1396:NSOTBJ>2.0.CO;2.

Yu, C.-K., and B. F. Smull, 2000: Airborne Doppler observations of a landfalling cold front upstream of steep coastal orography. *Mon. Wea. Rev.*, **128**, 1577–1603, doi:10.1175/1520-0493(2000)128<1577:ADOOAL>2.0.CO;2.